ARTICLE IN PRESS

Extreme Mechanics Letters ▮ (▮▮▮▮) ▮▮▮–▮▮▮

Contents lists available at ScienceDirect

Extreme Mechanics Letters

journal homepage: www.elsevier.com/locate/eml

Zero-frequency and extremely slow elastic edge waves in mechanical granular graphene

Li-Yang Zheng *, Vincent Tournat, Vitalyi Gusev *

LAUM, UMR-CNRS 6613, Universite du Maine, Av. O. Messiaen, 72085 Le Mans, France

ARTICLE INFO

Article history:
Received 29 February 2016
Received in revised form
9 August 2016
Accepted 19 August 2016
Available online xxxx

Keywords:
Granular phononic crystal
Zero-frequency modes
Slow edge waves

ABSTRACT

We report here the theoretical description and analysis of edge elastic waves in a semi-infinite mechanical granular graphene structure. The granular graphene, composed of spherical beads arranged in a single-layer honeycomb structure, is studied for two types of edge configurations: zigzag and armchair. Due to the existence of the rotational degrees of freedom of the grains, rotation-associated shear, bending and torsional couplings between the neighbor beads are activated. The dispersion curves of the edge waves are theoretically derived and numerically analyzed for various configurations of bead couplings, as well as the existence of edge states when the torsional or/and bending rigidities are weak/vanishing. Quasi-flat edge mode dispersion curves with near zero frequency are observed for both the zigzag and armchair edges. These quasi-flat dispersion curves, supporting the propagation of waves with extremely slow group velocity, tend to be perfect zero-frequency modes for zero torsional rigidity or vanish for zero bending rigidity, indicating that weak bending and torsional interbead interactions are critical in the transformation of zero-frequency modes into extremely slow propagating modes. These results on edge waves in mechanical granular graphene structures with rotational degrees of freedom are the necessary preliminary step for the design of granular meta-graphenes with artificial symmetry breaking for inducing topologically protected unidirectional edge states.

1. Introduction

Granular crystals are spatially periodic structures of particles, most often spherical homogeneous elastic beads, arranged in crystal lattices [1–17]. The beads are linked through their contacting areas or by interconnections, both of much smaller dimensions and weights than the ones of the beads, and the interactions between beads take place predominantly via normal and transverse rigidities of these elastic interconnections. In contrast to most of the mechanical systems where the interactions of neighboring particles can be mimicked by spring–mass models with central forces [18,19], in granular crystals, due to the non-central shear forces, rotation of individual beads can be initiated, and consequently the rotational degree of freedom (DOF) of the individual beads, the particle dimensions and the interactions through non-central forces cannot be ignored [5–8]. The analytical linear models accounting for the rotational DOFs have been derived for one-dimensional (1D) granular chains [9], two-dimensional (2D) granular membranes [10–13] and three-dimensional (3D) granular phononic crystals [14,15]. Because of the rotational DOFs of individual beads, it was theoretically reported [9–15] and experimentally tested [16,17] that in addition to the classical propagation modes, coupled rotational/transverse [16] and pure rotational modes [17] can be observed in granular crystals. Moreover, the existences of localized modes [9], zero-frequency modes and zero-group-velocity (ZGV) modes [11–13], the formation and manipulation of Dirac cones [13] have also been demonstrated in granular crystals.

In the last two decades, graphene, a monolayer of carbon atoms arranged in a 2D honeycomb lattice, has become one of the most fascinating objects in material sciences and condensed-matter physics [20–22]. Owing to its specific crystal symmetry, unusual energy band structure for charge carriers can be formed. An interesting consequence of a rich electronic spectrum is that the edge states may exist when boundaries are present. The existence of boundary, on one hand, breaks the crystal symmetry on the edges, but on the other hand, preserves some properties of the bulk, leading to the edge states having distinct propagation properties from the bulk modes and hence playing important roles in transport of electronic excitations [23–25]. For example, the zero modes (zero-frequency edge states) were theoretically

* Corresponding authors.
E-mail addresses: liyang.zheng.etu@univ-lemans.fr (L.-Y. Zheng), vitali.goussev@univ-lemans.fr (V. Gusev).

http://dx.doi.org/10.1016/j.eml.2016.08.003
2352-4316/

Please cite this article in press as: L.-Y. Zheng, et al., Zero-frequency and extremely slow elastic edge waves in mechanical granular graphene, Extreme Mechanics Letters (2016), http://dx.doi.org/10.1016/j.eml.2016.08.003

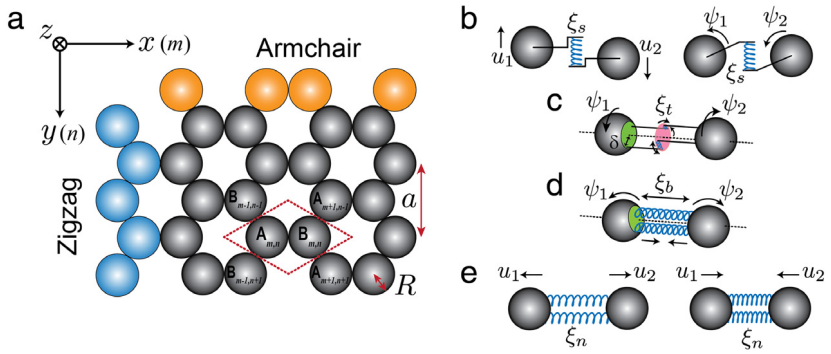

Fig. 1. Schematic presentation of the mechanical granular graphene and the possible intergrain interactions. (a) Structure of the considered graphene. Beads in blue label the zigzag edge and beads in orange label the armchair edge. (b) Shear forces activated by relative out-of-plane displacement and in-phase rotation of the adjacent beads. (c) Torsional forces induced by the resistance of contact to relative rotation of the beads along the axis connecting their centers. (d) Bending forces originated from the resistance of the contact to rolling of beads. (e) Normal forces providing the resistance to relative motion of the grains in the plane of the membrane. These forces do not contribute to the out-of-plane motion of the membrane, but their moments in (d) do contribute through initiating the rotations. (For interpretation of the references to color in this figure legend, the reader is referred to the web version of this article.)

and experimentally studied in graphene ribbons [26–33]. Even more interestingly, the quantum Hall effect (QHE) and quantum spin Hall effect (QSHE), where the topologically protected gapless edge states are robust channels for electronic transport, have been demonstrated [34–37].

Analogous to the above electron systems, the existence of edge state can emerge in completely different physical systems [38–50]. In the photonic/phononic analog of graphene, novel phenomena, such as zero-energy mode on the edge [41] and topological one-way edge states [42–45], have also been reported. However, in granular crystals, where most of the previous results addressed the structures of infinite size, only a few studies have considered the influence of a boundary. For instance, in 1D semi-infinite monatomic granular chains, the existence of localized modes have been theoretically demonstrated [9]. In 3D cubic granular crystals, the Rayleigh-type surface acoustic waves (SAWs) and shear-horizontal-type SAWs have been theoretically analyzed, and the existence of ZGV SAWs of Rayleigh-type has been predicted [14]. Recently for mechanical systems, the topologically protected one-way edge states which are unaffected by disorder were theoretically proposed [46,47] and experimentally observed [51] by breaking the time-reversal symmetry in the gyroscopic metamaterials, where the phononic analogue of the electronic quantum Hall effect is realized. Motivated by these recent results, the study of SAWs (or edge states) in 2D granular graphenes shows an interest as a necessary step towards their applications for elastic wave control through the design of artificially modified granular graphenes (granular meta-graphenes) where chiral or/and topological edge states become possible by the reduction of the symmetry of the membranes.

In this paper, we theoretically study the existence of edge states at the free boundaries of a semi-infinite mechanical granular graphene, which is a 2D homogeneous monolayer of elastic beads packed into a honeycomb lattice of lattice constant $a = 2\sqrt{3}R$ as shown in Fig. 1(a). An out-of-plane motion is imposed to the considered granular graphene with the zigzag and armchair boundaries. Consequently, each individual bead possesses one out-of-plane translational and two in-plane rotational DOFs and the mechanical contacts among them are provided by linear shear, bending and torsional rigidities, respectively, as depicted in Fig. 1(b)–(d). The dispersion curves of edge modes for varying bending/torsional rigidities are studied. Similar to the previous conclusions for the bulk mode [5,13], due to the rotational DOFs, the dispersion branches of edge modes can be modified by tuning the bending and torsional rigidities. On the other hand, we demonstrate that near zero-frequency modes may appear on both the zigzag and armchair edges when bending/torsional rigidities are weak. This result is different from the cases in electronic/photonic systems where zero-frequency modes do not exist on the armchair edge when the sublattices A and B are the same [26,31,41]. The physical origin of zero-frequency modes in the 2D granular monolayer honeycomb crystals has been interpreted in Ref. [13], where the zero-frequency mode results from the zero bending/torsional rigidities. In this work, we show that the existence of zero-frequency edge modes is also intimately related to the weakness of bending/torsional intergrain couplings.

It should be reminded here, that the possible existence of extremely slow waves in granular crystals relates to the fact that the interaction between the grains through the bending and torsional moments can be orders of magnitudes weaker than their interaction through the normal and shear forces. In non-consolidated granular crystals, the interactions between beads take place via local contacts, which are much smaller in size than the dimensions of the individual grains and effectively much softer than the beads' material [11–17]. Even when granular crystals are consolidated by curing, like opals, or by grain-connecting ligands, like in nanocrystal superlattices, the elastic links between the particles are still significantly smaller and softer than the grains themselves. This induces propagation of elastic waves in granular structures at significantly slower velocities than in the individual grains [4] even if the rotational DOFs of the individual beads are not strongly involved. Thus, in general granular crystals are much softer than the materials composing the individual grains. The granular crystals without rotational DOFs are theoretically modeled as spring–mass systems, where the spherical masses interact through forces transmitted by shear and normal springs with rigidities ξ_s and ξ_n respectively (see Fig. 1(b) and (e)). As the characteristic spatial scale in the granular crystal is of the order of grain radius, R, the characteristic frequencies of the vibrations can be estimated as being an order of $\sim\sqrt{\xi_{s,n}/M}$, respectively, where M is the mass of the grain, and the velocities of bulk acoustic waves are of the order, $\sim R\sqrt{\xi_{s,n}/M}$, respectively. As it has been explained above, because of the weakness of contact rigidities ξ_s and ξ_n, those bulk waves are much slower than the shear and longitudinal waves in the material composing the beads. When the rotational DOFs are taken into account, the rotations should be predominantly induced by shear springs, Fig. 1(b), which have the maximal possible arm equal to R for creating the grain-rotating moment. However, this is not always the case because under some circumstances simultaneous displacements and rotations of the grains could keep the shear springs unstrained [13]. In these situations, the interactions between the beads through the bending and torsional moments, which are much weaker than the

Please cite this article in press as: L.-Y. Zheng, et al., Zero-frequency and extremely slow elastic edge waves in mechanical granular graphene, Extreme Mechanics Letters (2016), http://dx.doi.org/10.1016/j.eml.2016.08.003

characteristic shear moments, could play an important role. As it is qualitatively illustrated in Fig. 1(c) and (d), the existence of both those moments is due to non-vanishing lateral size, $\delta \neq 0$, of the contacts/links between the grains. The shear and normal forces distributed in the cross-section of the contact/link provide the resistance to rotation of the beads in opposite directions relative to the axis connecting their centers (Fig. 1(c)) and relative to the axis normal to the centers connecting axis (Fig. 1(d)), respectively. However, both shear and normal forces distributed across the contact have very small arms, $\sim\delta \ll R$, for creating bead-rotating moments. The torsional and bending moments induced by the distributions of shear and normal forces, respectively, appear to be much smaller than the nominal moment that could be created by the shear spring in Fig. 1(b). For the estimates, the interactions through torsional and bending moments could be characterized by the corresponding characteristic torsional and bending rigidities, $\xi_t \sim \xi_s(\delta/R)^2$ and $\xi_b \sim \xi_n(\delta/R)^2$, respectively. Thus the waves which propagation is due to torsional/bending moment-type interaction between the neighbor grains will have the velocities $\sim\delta\sqrt{\xi_{s,n}/M} \ll R\sqrt{\xi_{s,n}/M}$ that are much slower than the velocities of classical acoustic waves in granular crystals which propagation is due to shear/normal force-type interactions. Correspondingly, these waves caused by torsional/bending interactions between the grains, could be considered as extremely slow in comparison with the acoustic waves propagating in the material composing the grains. Note that, commonly normal rigidity is comparable with shear rigidity, i.e., $\xi_n \geq \xi_s$, thus bending rigidity is comparable with torsional rigidity, $\xi_b \geq \xi_t$.

As it follows from the discussion above, for the realization of extremely slow waves in mechanical graphene the dimensions of the contacts between the spheres should be much smaller than the dimensions of the spheres. In non-cohesive granular crystals this conditions could be achieved in the regime of weak pre-compression [52–55]. For example recently the opportunity to modify the contact interaction between spheres by varying magnetic forces has been reported [52,53] and bending rigidities much smaller than the shear ones have been revealed. Otherwise the granular graphene could be potentially prepared by three-dimensional printing. If rod-type connections between the spheres are printed with dimensions much smaller than the sphere dimensions, then the effective torsional and bending rigidities of these artificially created contacts will be in general much weaker than their shear (normal) rigidities. It has been revealed that the weak bending and torsional forces/moments could be crucial in activating the propagation of some phonon modes [12,13]. Thus it is important and necessary to evaluate the role of the weak bending and torsional moments in granular crystals when their boundaries are investigated. Recently, in the studies of mechanical kagome network systems without the rotational DOFs of individual particles, it has been reported that the zero-frequency modes (topological soft modes) could exist [56–58]. Those modes are robust against a wide range of structural deformations or changes in material parameters, leading to potential applications for design/fabrication of soft materials [58,59]. The prediction of zero-frequency edge modes in granular crystals in the research work presented below can stimulate the exploration of zero-frequency mode in other mechanical system and pave the way towards engineering nanomechanical soft structures supporting propagation of extremely slow waves. In addition, we believe that our theoretical analysis of the elastic edge modes in mechanical granular graphenes with free boundary would be useful also in the studies of SAWs in the cases where the layers of microspheres are adhered to the elastic substrates [60,61].

The organization of this paper is as follows. In Section 2 the mechanical granular graphene is presented and the analytical model is described. The boundary conditions on the zigzag edge are introduced in Section 3, where the spectra of edge states and the zero-frequency modes are evaluated, presented and discussed. For the armchair type of boundary, the boundary conditions, the existence of edge states and zero-frequency edge modes are systematically examined in Section 4. Finally, we present the conclusions of this work in Section 5.

2. Model

The mechanical granular graphene presented in Fig. 1(a) exhibits two type of edges, zigzag and armchair, indicated in Fig. 1(a) by beads labeled in blue and orange, respectively. Considering the out-of-plane motion in the granular graphene, each individual bead exhibits the out-of-plane displacement (u) along z-axis and the in-plane rotational angles φ and ϕ (φ-rotation with the axis in the x-direction and ϕ-rotation with the axis in the y-direction). The dynamics and the couplings of these mechanical motions are controlled by the following forces and/or moments: (1) Shear forces, which are characterized by an effective shear rigidity ξ_s (Fig. 1(b)). These forces are activated in the graphene due to a resistance of the contact to relative displacement of the beads in the direction orthogonal to the axis connecting their centers and due to in-phase rotation of the beads relative to the direction orthogonal to the axis connecting their centers. (2) Torsional forces, which are characterized by an effective torsional (spin) rigidity ξ_t (Fig. 1(c)). The resistance of the contact to relative rotation of the beads along the axis connecting their centers can initiate these forces. (3) Bending forces, which are characterized by an effective bending rigidity ξ_b (Fig. 1(d)). They originate from the resistance of the beads contact to rolling.

We label the sublattice A (B) in the normalized coordinate (m, n) by $A_{m,n}$ ($B_{m,n}$), as shown in Fig. 1(a), where m and n are both integers. According to the analysis in Ref. [13], the dynamical equations on site (m, n) are given by,

$$S_{\text{out}}(q_x, q_y)\vec{v}_{\text{out}} = \begin{bmatrix} Q & U \\ N & Q \end{bmatrix} \begin{bmatrix} v_A \\ v_B \end{bmatrix} = \widehat{0}, \tag{1}$$

where $v_A = (u^A, \Phi^A, \Psi^A)^T$ and $v_B = (u^B, \Phi^B, \Psi^B)^T$ with $\Phi = R\varphi$, $\Psi = R\phi$ and the superscript T represents the transposed vector. Q, U and N are 3×3 matrices (see the details in Appendix A). For non-trivial solutions, the following condition should be satisfied,

$$\det|S_{\text{out}}(q_x, q_y)| = 0. \tag{2}$$

Solution of the eigenvalue problem in Eqs. (1) gives the dispersion curves of the bulk modes described in Ref. [13], which are not shown in this work as our main goal is the description of edge modes.

3. Zigzag edge

In this section, the boundary conditions of the mechanically free zigzag edge of the granular graphene, as highlighted by blue beads in Fig. 1(a), are derived. Assuming the granular graphene is semi-infinite and the zigzag edge is introduced on site $(0, n)$ by removing the beads $A_{0,n}$ and those with $m < 0$, the boundary conditions are derived from the cancellation of the interactions between the removed grains $A_{0,n}$ and the edge grains $B_{0,n}$. For example, on site $(0, 0)$ the interplays between sublattice $A_{0,0}$ and $B_{0,0}$ should be zero, thus the boundary conditions are written as,

$$u^A_{0,0} - u^B_{0,0} + (\Psi^A_{0,0} + \Psi^B_{0,0}) = 0, \tag{3a}$$

$$\eta_t(\Phi^A_{0,0} - \Phi^B_{0,0}) = 0, \tag{3b}$$

$$\eta_b(\Psi^A_{0,0} - \Psi^B_{0,0}) = 0, \tag{3c}$$

Please cite this article in press as: L.-Y. Zheng, et al., Zero-frequency and extremely slow elastic edge waves in mechanical granular graphene, Extreme Mechanics Letters (2016), http://dx.doi.org/10.1016/j.eml.2016.08.003

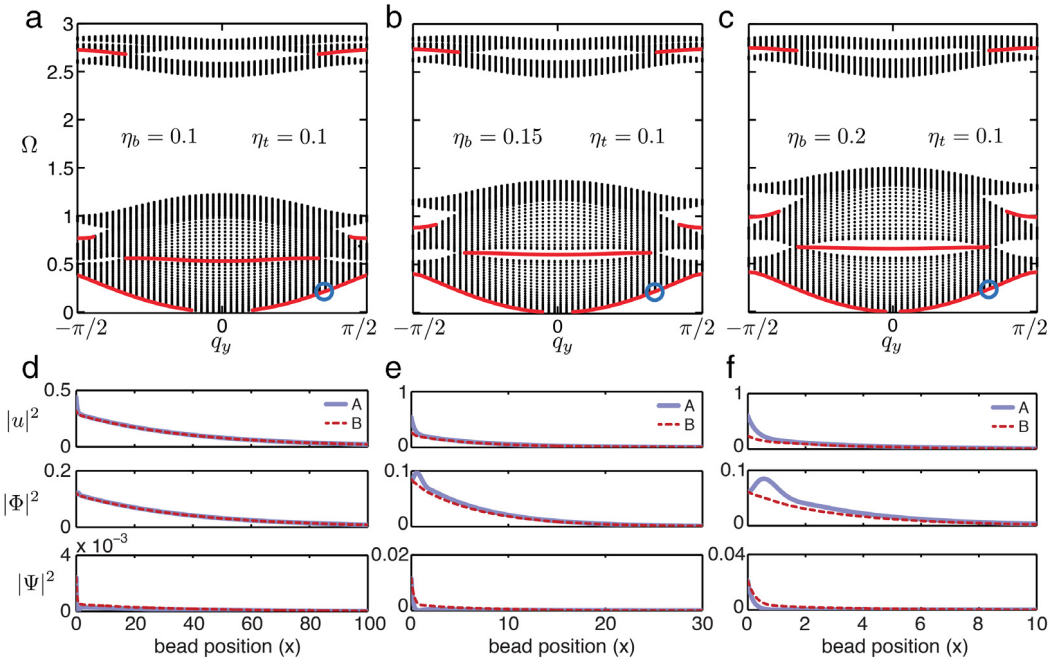

Fig. 2. The projected band structures along q_y direction of the graphene for $\eta_t = 0.1$ and $\eta_b = 0.1$ (a), $\eta_b = 0.15$ (b) and $\eta_b = 0.2$ (c). The black dot areas represent the projected bulk bands along y-direction, and the red curves represent the edge states. The amplitudes of three components u, Φ and Ψ of the edge state at point $q_y = \pi/3$ (labeled by blue circles in (a)–(c)) as a function of bead position along x-direction are shown for $\eta_t = 0.1$ and $\eta_b = 0.1$ (d), $\eta_b = 0.15$ (e) and $\eta_b = 0.2$ (f). The blue curves correspond to sublattice A and the red dash curves to sublattice B. (For interpretation of the references to color in this figure legend, the reader is referred to the web version of this article.)

where $\eta_b = \xi_b/\xi_s$ ($\eta_t = \xi_t/\xi_s$) denotes the ratio of bending (torsional) to shear rigidity. For waves associated with the free boundary $m = 0$, we are looking for the solution of the form [14],

$$(u^A, \Phi^A, \Psi^A)_{\text{zig}} = \sum_{j=1}^{3} (\alpha_j^A, \beta_j^A, \gamma_j^A) K_j e^{i\omega t - mq_{xj} - nq_y}, \tag{4a}$$

$$(u^B, \Phi^B, \Psi^B)_{\text{zig}} = \sum_{j=1}^{3} (\alpha_j^B, \beta_j^B, \gamma_j^B) K_j e^{i\omega t - mq_{xj} - nq_y}, \tag{4b}$$

where α_j, β_j and γ_j (see Appendix B for more details) are three factors determining the composition of bulk eigenmodes, K_j are constants. Substituting Eqs. (4) into Eqs. (3), the boundary conditions can be rewritten in the matrix form,

$$S_{\text{zig}}(q_{xj}, q_y)\vec{K}_{\text{zig}} = 0, \tag{5}$$

where $S_{\text{zig}}(q_{xj}, q_y)$ is the boundary condition matrix of zigzag edge and $\vec{K}_{\text{zig}}$ is the eigenvector of the boundary matrix. The details of the derivation of the boundary matrix are presented in Appendix B. For nontrivial solutions, the determinant of the boundary matrix must be zero,

$$\det|S_{\text{zig}}(q_{xj}, q_y)| = 0. \tag{6}$$

Combining Eqs. (2) and (6), the solutions of the zigzag edge are obtained.

3.1. Edge modes

In this section, the $\Omega - k$ dispersion curves of the edge modes for different values of the ratios η_b and η_t are derived. Without loss of generality, in Fig. 2 we present the projected band structures, where the bulk modes of the first Brillouin zone have been projected into the q_y direction in the reciprocal space, for the case of a fixed $\eta_t = 0.1$ and a varying η_b. As shown in Fig. 2, the bulk modes are concentrated mainly in two separated areas. The low frequency area, containing three lowest bulk bands, is defined as lower-frequency phonon area (LPA) and the high frequency area, composed of three highest bulk bands, is noted as higher-frequency phonon area (HPA). There exists a large band gap between the LPA and HPA due to the fact that bending/torsional rigidities are much smaller than shear rigidities. For increasing bending/torsional rigidities, this band gap is squeezed. Dirac cones are observed at $q_y = \pm\pi/3$ in the LPA and HPA as shown in Fig. 2(a)–(c). In general, four branches of edge modes are obtained, labeled as red lines in Fig. 2(a)–(c), three of which are located in the LPA and another one in the HPA. Tuning the bending and torsional rigidities of contact is possible to control the propagation properties of the edge modes. For example, in the case of $\eta_b = 0.1$ and $\eta_t = 0.1$, the edge band below the first propagative bulk band is located very close to the bulk band, leading to edge modes possessing properties similar to those of the bulk modes. The amplitudes of the three components u, Φ and Ψ for wave vector $q_y = \pi/3$ highlighted in Fig. 2(a) are shown as a function of bead position along the bulk direction, as shown in Fig. 2(d), where the blue curves correspond to beads A and the red dash curves to beads B. It implies that the edge mode exhibits weak in-depth localization as the oscillations of the beads spread into the bulk for a rather long distance. When increasing η_b to 0.15, as shown in Fig. 2(b), the edge mode of the wave vector $q_y = \pi/3$ is easier to distinguish from the bulk modes than that of $\eta_b = 0.1$ in the projected diagram, thus the edge state becomes more localized and its penetration depth into the bulk is shorter (Fig. 2(e)). For $\eta_b = 0.2$ in Fig. 2(c), the edge mode with $q_y = \pi/3$ has very distinct properties from the bulk mode, leading to the motion of beads localized only on a few layers near the free boundary as shown in Fig. 2(f). These controllable properties of edge state suggest that the bending/torsional couplings are crucial in the propagation of elastic edge waves belonging to the LPA.

In the following, we discuss the influence of weak torsional or/and bending couplings on the in-depth localized modes propagating along the free zigzag edge.

Please cite this article in press as: L.-Y. Zheng, et al., Zero-frequency and extremely slow elastic edge waves in mechanical granular graphene, Extreme Mechanics Letters (2016), http://dx.doi.org/10.1016/j.eml.2016.08.003

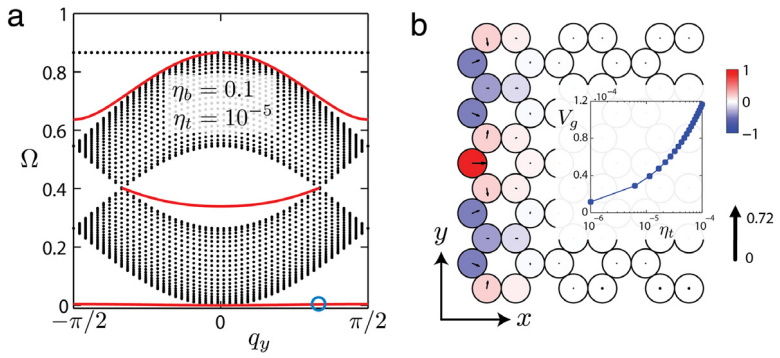

Fig. 3. (a) Dispersion curves of edge states for $\eta_b = 0.1$ and $\eta_t = 10^{-5}$ in LPA. A quasi-flat band with near zero frequency can be observed. (b) Movement of beads of the near-zero-frequency mode at point $q_y = \pi/3$ highlighted in (a) by a blue circle. The insert shows the relation between the normalized group velocity of near-zero-frequency modes for a fixed wave vector $q_y = \pi/3$ and normalized torsional rigidity η_t. The amplitude of the out-of-plane displacement of each bead is normalized. Thus the color marked on each bead represents the amplitude of displacement which can be read from the color bar. The orientation of arrows represents the rotating directions of beads. The length of arrows, which is normalized to the longest arrows whose amplitudes are shown in the arrow bar, represents the amplitude of rotations of beads. (For interpretation of the references to color in this figure legend, the reader is referred to the web version of this article.)

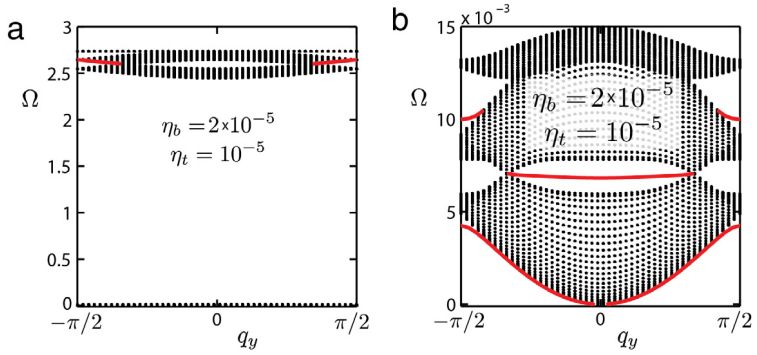

Fig. 4. The projected band structure of granular graphene along the q_y direction for $\eta_b = 2 \times 10^{-5}$ and $\eta_t = 10^{-5}$. (a) One band of edge state exists in the HPA, while the bands of bulk modes in the LPA collapse into a narrow frequency zone. (b) The zoomed view of the LPA. Three bands of edge state can be observed in this area.

3.2. Zero-frequency modes

In this section, we first discuss the case of weak torsional rigidity only, and later we turn to the influence of both weak bending and weak torsional rigidities under the condition that $\xi_b \geq \xi_t$. When torsional moments are weak, for example $\eta_t = 10^{-5}$ while $\eta_b = 0.1$, the dispersion curves of edge state represented by red curves in LPA are shown in Fig. 3(a). It is clearly seen that the edge branch below the first propagating bulk area is a quasi-flat band with near zero frequency. We choose the point of $q_y = \pi/3$ (labeled by blue circle in Fig. 3(a)) to analyze the near-zero-frequency mode. The movements of beads are shown in Fig. 3(b), where different colors of beads represent the different out-of-plane, i.e. along the z-axis, displacement of beads and the amplitude of displacement of beads is presented by the color bar. The rotational axis of each bead are presented by the arrow marked on beads and the amplitudes of rotation are normalized to the maximum value in the arrow bar, thus the length of arrows marked on the beads represent the amplitude of rotations. It is clearly shown that the oscillation of beads are localized mainly on the first three layers near the edge. The existence of zero-frequency mode has been reported in many systems and a criterion to determine the existence of zero-frequency edge modes has also been established in terms of bulk properties and the chiral symmetry [29,41,53]. In granular crystals, the existence of zero-frequency mode and their transitions into slow mode strongly rely on the rotational interactions of beads [13]. For example, the insert in Fig. 3(b) reveals the relation between the torsional rigidity and the normalized group velocity of the near-zero-frequency modes ($V_g = v_g \cdot 2/(3\omega_0 R)$, where v_g is the group velocity and $\omega_0 = \sqrt{\xi_s/M}$ is the characteristic frequency provided by the magnitude of shear rigidity) when the wave vector is fixed at $q_y = \pi/3$. It suggests that the group velocity of edge states is extremely slow when torsional rigidity is weak. The results presented in the insert in Fig. 3 confirm that acoustic waves supported by the weak torsional rigidity could be of several orders of magnitude slower than such acoustic waves supported by the shear rigidity of the contacts as, for example, longitudinal and transverse bulk acoustic modes evaluated in the granular crystals neglecting rotational degrees of freedom. The smaller the torsional rigidity is, the closer to zero the group velocity of the near-zero-frequency modes is. As torsional rigidity is closer and closer to zero, this quasi-flat band tends to become a perfectly non-propagative flat band at zero frequency. For non-zero finite torsional rigidity, zero-frequency non-propagating edge modes are transformed into slow modes with low group velocity.

When both bending and torsional rigidities are small, near-zero-frequency edge modes can be also obtained. For example, for $\eta_b = 2 \times 10^{-5}$ and $\eta_t = 10^{-5}$, the dispersion diagram of edge state is depicted in Fig. 4(a), where three low frequency bulk bands are collapsed into the narrow zone with near zero frequency. This is due to the simultaneously small values of bending and torsional rigidity [13]. Nevertheless, the existence of edge state in the LPA can be still evaluated. The zoom-in of the low frequency bulk bands is shown in Fig. 4(b), where three branches of edge state are observed. The edge states inside this extremely low frequency zone behave as the ones in the quasi-flat bands with near zero frequency. As predicted in Ref. [13], when the bending rigidity is zero, the bulk bands in the LPA collapse into three degenerated zero-frequency bands. One could expect that the associated edge states, which in Fig. 4(b) are confined either between the bulk bands or between the lowest bulk band and the zero frequency, would eventually vanish for zero bending rigidity. For weak but

Please cite this article in press as: L.-Y. Zheng, et al., Zero-frequency and extremely slow elastic edge waves in mechanical granular graphene, Extreme Mechanics Letters (2016), http://dx.doi.org/10.1016/j.eml.2016.08.003

non-zero bending/torsional rigidities, the three degenerated zero-frequency bulk branches are transformed into three slow wave bands, resulting in the existence of near-zero-frequency edge modes with extremely slow group velocity, Fig. 4(b).

4. Armchair edge

The mechanical granular graphene with the free armchair edge is illustrated in Fig. 1(a) highlighted in orange beads. Assuming the armchair edge is on site $(m, 0)$ by removing all the beads with $n < 0$, the boundary conditions are derived from the absence of the interbead interactions between the cut layer $(m, -1)$ and the edge layer $(m, 0)$. For example, on site $(0, 0)$, the interactions between the beads $A_{0,0}$ $(B_{0,0})$ and $B_{-1,-1}$ $(A_{1,-1})$ should be zero, thus the boundary conditions are obtained,

$$2(u^B_{-1,-1} - u^A_{0,0}) - \sqrt{3}(\Phi^B_{-1,-1} + \Phi^A_{0,0}) + (\Psi^B_{-1,-1} + \Psi^A_{0,0}) = 0, \tag{7a}$$

$$\eta_t(\Phi^B_{-1,-1} - \Phi^A_{0,0}) + \sqrt{3}\eta_t(\Psi^B_{-1,-1} - \Psi^A_{0,0}) = 0, \tag{7b}$$

$$-\sqrt{3}\eta_b(\Phi^B_{-1,-1} - \Phi^A_{0,0}) + \eta_b(\Psi^B_{-1,-1} - \Psi^A_{0,0}) = 0, \tag{7c}$$

$$2(u^A_{1,-1} - u^B_{0,0}) - \sqrt{3}(\Phi^A_{1,-1} + \Phi^B_{0,0}) - (\Psi^A_{1,-1} + \Psi^B_{0,0}) = 0, \tag{7d}$$

$$\eta_t(\Phi^A_{1,-1} - \Phi^B_{0,0}) - \sqrt{3}\eta_t(\Psi^A_{1,-1} - \Psi^B_{0,0}) = 0, \tag{7e}$$

$$\sqrt{3}\eta_b(\Phi^A_{1,-1} - \Phi^B_{0,0}) + \eta_b(\Psi^A_{1,-1} - \Psi^B_{0,0}) = 0. \tag{7f}$$

For the wave propagating along the armchair edge, we seek a solution of the form,

$$(u^A, \Phi^A, \Psi^A)_{\text{arm}} = \sum_{j=1}^{6}(\alpha^A_j, \beta^A_j, \gamma^A_j)K_j e^{i\omega t - mq_x - nq_{yj}}, \tag{8a}$$

$$(u^B, \Phi^B, \Psi^B)_{\text{arm}} = \sum_{j=1}^{6}(\alpha^B_j, \beta^B_j, \gamma^B_j)K_j e^{i\omega t - mq_x - nq_{yj}}. \tag{8b}$$

Substituting Eqs. (8) into Eqs. (7), the boundary conditions can be rewritten in the matrix form,

$$S_{\text{arm}}(q_x, q_{yj})\vec{K}_{\text{arm}} = 0, \tag{9}$$

where $S_{\text{arm}}(q_x, q_{yj})$ is the boundary condition matrix of armchair edge and $\vec{K}_{\text{arm}}$ is the eigenvector of the boundary matrix. More information about the calculation of the boundary matrix can be found in Appendix C. For nontrivial solutions, the determinant of the boundary matrix must satisfy the following relation,

$$\det|S_{\text{arm}}(q_x, q_{yj})| = 0. \tag{10}$$

The solutions for the edge mode of armchair edge are computed by combining Eqs. (2) and (10).

4.1. Edge modes

In this section, the $\Omega - k$ projected band structures for different values of the parameters η_b and η_t are derived. It is shown that it is possible to modify the dispersion diagram by a fine tuning of the contact rigidities. For example, the dispersion curves of the edge states for a fixed $\eta_b = 0.4$ but a changing η_t are depicted in Fig. 5, where edge modes are labeled as red curves and the black dot areas represent the bulk modes. The particular number of existing edge bands depends on the value of η_t. Explicitly, for

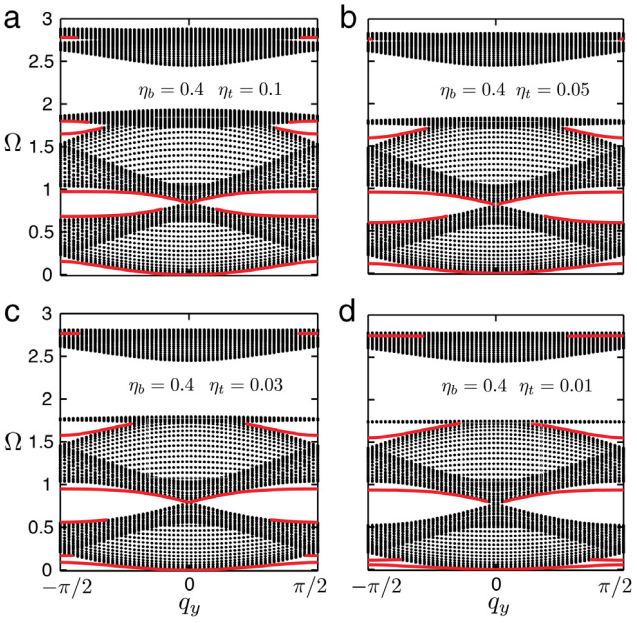

Fig. 5. Dispersion diagrams for the armchair boundary for a fixed $\eta_b = 0.4$ but $\eta_t = 0.1$ (a), $\eta_t = 0.05$ (b), $\eta_t = 0.03$ (c) and $\eta_t = 0.01$ (d). Red curves correspond to the edge states and the black dot areas represent projected bulk modes. (For interpretation of the references to color in this figure legend, the reader is referred to the web version of this article.)

modes in the LPA, Fig. 5(a) shows the dispersion curves for $\eta_b = 0.4$ and $\eta_t = 0.1$. Two edge bands appear between the second and third bulk bands. When the value of η_t decreases to 0.05, one of these edge bands disappears, as shown in Fig. 5(b). Continuing to decrease η_t to 0.03, one new edge band appears in each of the regions below the first bulk band as presented in Fig. 5(c). Reducing η_t to 0.01, Fig. 5(d), one of the edge bands which existed between the first and second bulk bands vanishes. We can predict that, in the LPA, in the regions between the third and second bulk bands, between the second and the first bulk bands, and below the first bulk band there always exists at least one edge band in each region, while one additional edge band may appear in each of these regions depending on the bending and torsional rigidities. Similar phenomena of variation of the number of edge bands have also been found in the HPA of the dispersion diagram. For example, when η_t changes from 0.1 to 0.01, the edge band in HPA would disappear and reappear. Those controllable features of edge states by tuning bending and torsional rigidities provide extra flexibilities in the design of functional devices for elastic wave transport based on granular crystals.

4.2. Zero-frequency modes

In this section, we first investigate the case of weak torsional coupling only, and later we discuss the influence of both weak bending and torsional couplings under the condition that $\xi_b \geq \xi_t$.

For very small value of η_t, the quasi-flat bands of edge modes at near zero frequency may appear in the projected dispersion diagram. Fig. 6 shows the dispersion curves of edge state for $\eta_b = 0.2$ and $\eta_t = 10^{-5}$. These exists a near-zero-frequency band and a quasi-flat band of non-zero frequency just above it. We study the edge modes of $q_x \approx \pi/4$ (labeled by blue circles in Fig. 6(a)). The corresponding movements of beads are demonstrated in Fig. 6(b) and (c). It is clearly seen that the edge waves are propagating along x-axis being in-depth localized mostly on just a few layers near the edge. The insert in Fig. 6(a) shows the normalized group velocity ($V_g = v_g \cdot 2/(3\omega_0 R)$) of the first (near-zero-frequency) and the second (non-zero-frequency) quasi-flat modes as a function of

Please cite this article in press as: L.-Y. Zheng, et al., Zero-frequency and extremely slow elastic edge waves in mechanical granular graphene, Extreme Mechanics Letters (2016), http://dx.doi.org/10.1016/j.eml.2016.08.003

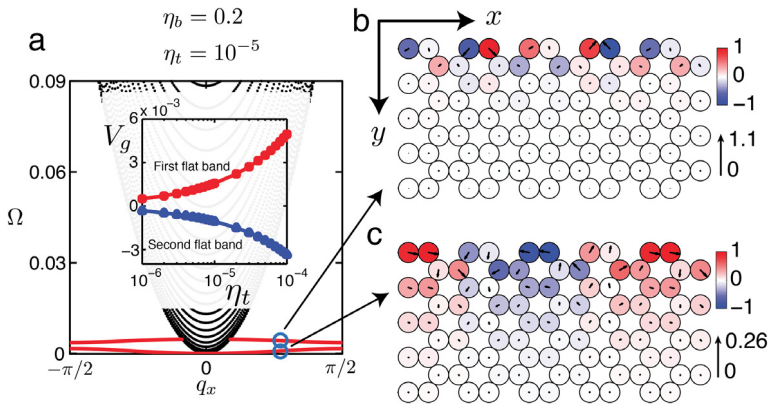

Fig. 6. (a) The dispersion curves of edge modes with slow velocity for $\eta_b = 0.2$ and $\eta_t = 10^{-5}$. Two quasi-flat bands appear when torsional rigidity is weak. The corresponding movements of beads for the wave vector $q_x \approx \pi/4$ noted by the blue circles are shown in (b) and (c). (b) The oscillation of beads on the edge for the second quasi-flat band. (c) The corresponding oscillation of edge state for the first quasi-flat band. The insert scheme in (a) illustrates the variations of group velocity of the quasi-flat bands as a function of η_t. (For interpretation of the references to color in this figure legend, the reader is referred to the web version of this article.)

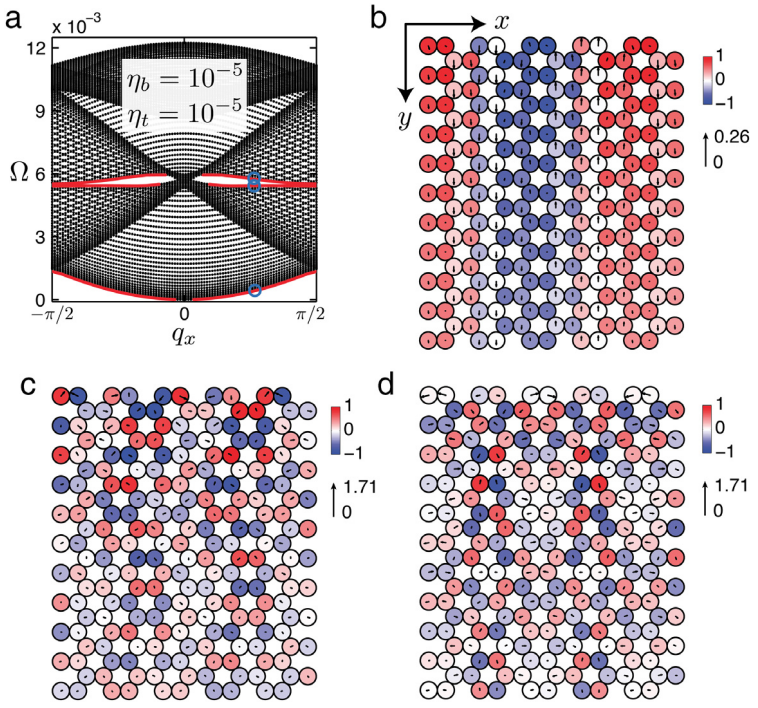

Fig. 7. The dispersion curves of edge modes in the LPA for $\eta_b = \eta_t = 10^{-5}$ and the corresponding movements of the beads with vector $q_x \approx \pi/4$ highlighted by blue circles in (a). (a) Dispersion curves of edge states. Three branches, presented as red curves, are found in the LPA. The oscillation for $q_x \approx \pi/4$ of the first (b), second (c) and third (d) edge bands are depicted. These edge states can penetrate into the bulk for a rather long distance. (For interpretation of the references to color in this figure legend, the reader is referred to the web version of this article.)

η_t. Note that the normalized group velocity in the first band has opposite sign to the one in the second branch. Principally, both bands have very slow velocity when the torsional rigidity is weak. For the extreme case when torsional rigidity tends to zero, both bands have the tendency to be perfect flat bands at zero frequency supporting non-propagative edge modes. Similar to the results on zigzag edge, weak torsional rigidity can initiate the propagation of zero-frequency modes by transforming them into slow modes.

When both bending and torsional rigidity are weak, near-zero-frequency modes also can be found as shown in Fig. 7(a), where the dispersion curves of the LPA for $\eta_b = \eta_t = 10^{-5}$ are exhibited. Similar to the case of the zigzag edge, the small value of bending rigidity can lead to collapse of projected bulk bands into the region close to zero frequency, thus the associated edge states are confined to a very narrow low frequency zone. In this case, the dispersion curves of edge modes are very close to the bulk bands, resulting in edge states exhibiting weak in-depth localization. For example, we analyzed the edge waves with wave vector $q_x \approx \pi/4$ marked by the blue circles in Fig. 7(a). The corresponding movements of beads in those three bands are shown in Fig. 7(b)–(d). As explained in Section 3.1, the closer the position of edge band is located to the bulk band, the weaker in-depth localization of the edge modes is. This prediction is valid in Fig. 7(b)–(d) where those three edge states of $q_x \approx \pi/4$ are weakly localized in-depth along the bulk. Similar to the results on the zigzag edge, for zero bending rigidity, slow edge modes in the LPA disappear.

5. Conclusion

In this work, we theoretically studied the existence of edge states with out-of-plane motion on the free zigzag and armchair boundaries of 2D semi-infinite mechanical granular graphenes.

Please cite this article in press as: L.-Y. Zheng, et al., Zero-frequency and extremely slow elastic edge waves in mechanical granular graphene, Extreme Mechanics Letters (2016), http://dx.doi.org/10.1016/j.eml.2016.08.003

Due to the additional rotational DOFs, the bending and torsional moments can be initiated between adjacent beads. By modifying the bending and torsional rigidities of contact, one could manipulate the dispersion of the edge states. Although the bending/torsional rigidities are weak in granular crystals, we demonstrate that they are crucial for the existence of slow propagating near zero-frequency modes on both zigzag and armchair edges. When torsional rigidity is weak, the extremely slow near-zero-frequency edge modes, whose group velocity depends on the torsional rigidity, exist on both zigzag and armchair edges. When bending rigidity also becomes weak in addition to torsional one, edge states in the LPA of the dispersion diagram are localized very close to zero frequency. Due to the fact that they are very close to the bulk modes in the dispersion diagram, edge modes in this case can be weakly localized in depth. For weak torsional rigidity, the quasi-flat bands at near zero frequency transform into the perfect zero-frequency edge modes when torsional rigidity tends to zero, while for weak bending rigidity, those edge modes show the tendency of vanishing as bending rigidity is further reduced. The granular graphene membrane could be, in principle, prepared by three-dimensional printing. In accordance with the theoretical estimations [13,14], intersphere connections, where bending and torsional rigidities are much weaker than shear one, could be prepared if the dimensions of the contacts are much smaller than the radius of the sphere. There are also possibilities to assemble a granular graphene supporting the propagation of slow elastic edge waves manually. The elastic spheres discussed in this article could be in macro scale, which means that the particles can be displaced manually and the structure can be practically assembled nearly perfectly with almost zero disorder and missing contacts [52,53]. For example, in Ref. [53], when the external force (pre-compression) achieved through the magnetic interaction between the spheres is around $4N$, the wave dynamics is linear and the magnitude of bending rigidity is around 5 orders of magnitude smaller than the shear rigidity, which is exactly the same order of magnitude that was assumed for some of the estimates in our work. Therefore, assembling magnetic beads nearly perfectly in the geometry of the granular graphene and achieving weak bending and torsional interactions is potentially possible. An adapted shaker attached to beads on the edge can be used as the source in the view to initiate the different motions of the beads. Particle acceleration can be recorded by using small accelerometers glued to the side of several beads or by laser vibrometer measurements. The physical realizations of the described granular graphene are of interest in devices of signal processing using acoustic waves and in the design of acoustic delay lines. In this article, the investigation of edge modes in mechanical granular graphene could in turn provide considerable insights into their optical/acoustic graphene analogues. The study of the near-zero-frequency modes caused by the existence of weak rotational interactions is useful for the potential realistic design of granular crystals supporting controllable propagation of extremely slow edge waves. In addition, it paves the way for the analysis of a variety of possible modifications of the above presented granular graphene with the goal of designing granular metamaterials supporting one-way propagating edge states.

Acknowledgments

This work was supported by the fellowship of China Scholarship Council for L.-Y. Zheng and carried out in the frame of the project ⟨Pari scientifique PROPASYM⟩ funded by Region Pays-de-la-Loire. We also acknowledge fruitful discussions with Dr. Hélène Pichard from ESPCI ParisTech, and Professors Ming-Hui Lu and Yan-Feng Chen from College of Engineering and Applied Sciences, Nanjing University, Nanjing, Jiangsu, China.

Appendix A. Dynamical equations for the bulk modes

According to Ref. [13], one can obtain the dynamical equations for the bulk modes,

$$S_{\text{out}}(q_x, q_y)\vec{v}_{\text{out}} = \begin{bmatrix} Q & U \\ N & Q \end{bmatrix} \begin{bmatrix} v_A \\ v_B \end{bmatrix} = \widehat{0}, \tag{A.1}$$

where Q, U and N are 3×3 matrices of the forms in Eqs. (A.2)–(A.4) as given in Box I. $\mathrm{P} = MR^2/I$ is the ratio of mass to inertia of beads and $q_x = 3k_x a/4$, $q_y = \sqrt{3}k_y a/4$ are the normalized wave vectors for k_x, k_y, respectively. $\Omega = \omega/\omega_0$ is the normalized frequency with $\omega_0 = \sqrt{\xi_s/M}$. $\eta_b = \xi_b/\xi_s$ ($\eta_t = \xi_t/\xi_s$) denotes the ratio of bending (torsional) to shear rigidity.

Appendix B. Boundary condition matrix of zigzag edge

According to Appendix A, the dynamical equation lead to the relations,

$$v_A = Q^{-1}(-U)v_B = S_A v_B, \tag{B.1a}$$

$$(NS_A + Q)v_B = S_B v_B = \widehat{0}, \tag{B.1b}$$

where S_A and S_B are 3×3 matrices. Assuming the solution to the dynamical equations has the form of a plane wave, thus,

$$v_A = (u^A, \Phi^A, \Psi^A)^T = (\alpha^A, \beta^A, \gamma^A)^T K e^{i\omega t - mq_x - nq_y}, \tag{B.2a}$$

$$v_B = (u^B, \Phi^B, \Psi^B)^T = (\alpha^B, \beta^B, \gamma^B)^T K e^{i\omega t - mq_x - nq_y}, \tag{B.2b}$$

with the relations,

$$\alpha^B = S_B^{(3,3)} S_B^{(2,2)} - S_B^{(3,2)} S_B^{(2,3)}, \tag{B.3a}$$

$$\beta^B = S_B^{(3,1)} S_B^{(2,3)} - S_B^{(3,3)} S_B^{(2,1)}, \tag{B.3b}$$

$$\gamma^B = S_B^{(3,2)} S_B^{(2,1)} - S_B^{(3,1)} S_B^{(2,2)}. \tag{B.3c}$$

Considering the edge states on the free zigzag boundary, we are looking for the solutions of the form in Eqs. (4). Substituting Eqs. (4) into the boundary conditions Eqs. (3), one could directly obtain the relations,

$$\sum_{j=1}^{3} \left(\alpha_j^A - \alpha_j^B + \gamma_j^A + \gamma_j^B\right) K_j = 0, \tag{B.4a}$$

$$\sum_{j=1}^{3} \left(\beta_j^A - \beta_j^B\right) K_j = 0, \tag{B.4b}$$

$$\sum_{j=1}^{3} \left(\gamma_j^A - \gamma_j^B\right) K_j = 0, \tag{B.4c}$$

which can be rewritten in the following form,

$$S_{\text{zig}}(q_{xj}, q_y)\vec{K}_{\text{zig}} = 0. \tag{B.5}$$

In Eq. (B.5) $\vec{K}_{\text{zig}} = (K_1, K_2, K_3)^T$ is the eigenvector of the boundary matrix, and $S_{\text{zig}}(q_{xj}, q_y)$ is the boundary condition matrix of zigzag edge, which is of the form, see Box II.

For the existence of the nontrivial solutions, the following equation must be satisfied,

$$\det|S_{\text{zig}}(q_{xj}, q_y)| = 0. \tag{B.7}$$

The dispersion relations of edge waves can be obtained.

Please cite this article in press as: L.-Y. Zheng, et al., Zero-frequency and extremely slow elastic edge waves in mechanical granular graphene, Extreme Mechanics Letters (2016), http://dx.doi.org/10.1016/j.eml.2016.08.003

$$Q = \begin{bmatrix} 3-\Omega^2 & 0 & 0 \\ 0 & \dfrac{3(1+\eta_b+\eta_t)}{2} - \dfrac{\Omega^2}{\mathrm{P}} & 0 \\ 0 & 0 & \dfrac{3(1+\eta_b+\eta_t)}{2} - \dfrac{\Omega^2}{\mathrm{P}} \end{bmatrix} \tag{A.2}$$

$$U = \begin{bmatrix} -1-2e^{iq_x}\cos q_y & \sqrt{3}ie^{iq_x}\sin q_y & 1-e^{iq_x}\cos q_y \\ -\sqrt{3}ie^{iq_x}\sin q_y & \dfrac{3-3\eta_b-\eta_t}{2}e^{iq_x}\cos q_y - \eta_t & -\dfrac{\sqrt{3}(1-\eta_b+\eta_t)}{2}ie^{iq_x}\sin q_y \\ e^{iq_x}\cos q_y - 1 & -\dfrac{\sqrt{3}(1-\eta_b+\eta_t)}{2}ie^{iq_x}\sin q_y & \dfrac{1-\eta_b-3\eta_t}{2}e^{iq_x}\cos q_y + 1 - \eta_b \end{bmatrix} \tag{A.3}$$

$$N = \begin{bmatrix} -1-2e^{-iq_x}\cos q_y & \sqrt{3}ie^{-iq_x}\sin q_y & e^{-iq_x}\cos q_y - 1 \\ -\sqrt{3}ie^{-iq_x}\sin q_y & \dfrac{3-3\eta_b-\eta_t}{2}e^{-iq_x}\cos q_y - \eta_t & \dfrac{\sqrt{3}(1-\eta_b+\eta_t)}{2}ie^{-iq_x}\sin q_y \\ 1-e^{-iq_x}\cos q_y & \dfrac{\sqrt{3}(1-\eta_b+\eta_t)}{2}ie^{-iq_x}\sin q_y & \dfrac{1-\eta_b-3\eta_t}{2}e^{-iq_x}\cos q_y + 1 - \eta_b \end{bmatrix}. \tag{A.4}$$

Box I.

$$S_{\mathrm{zig}}(q_{xj}, q_y) = \begin{bmatrix} \alpha_1^A - \alpha_1^B + \gamma_1^A + \gamma_1^B & \alpha_2^A - \alpha_2^B + \gamma_2^A + \gamma_2^B & \alpha_3^A - \alpha_3^B + \gamma_3^A + \gamma_3^B \\ \beta_1^A - \beta_1^B & \beta_2^A - \beta_2^B & \beta_3^A - \beta_3^B \\ \gamma_1^A - \gamma_1^B & \gamma_2^A - \gamma_2^B & \gamma_3^A - \gamma_3^B \end{bmatrix}. \tag{B.6}$$

Box II.

Appendix C. Boundary condition matrix of armchair edge

Considering the edge states on the free armchair boundary, the solutions of edge states have the form in Eqs. (8). Substituting Eqs. (8) into the boundary conditions Eqs. (7), one could directly obtain the boundary condition matrix,

$$S_{\mathrm{arm}}(q_x, q_{yj})\vec{K}_{\mathrm{arm}} = 0, \tag{C.1}$$

where $\vec{K}_{\mathrm{arm}} = (K_1, K_2, K_3, K_4, K_5, K_6)^T$ and S_{arm} is a 6×6 matrix composed of the following elements,

$$S_{\mathrm{arm}}^{(1,j)} = -2\alpha_j^A - \sqrt{3}\beta_j^A + \gamma_j^A c + (2\alpha_j^2 - \sqrt{3}\beta_j^B + \gamma_j^B)e^{i(q_x+q_{yj})}, \tag{C.2a}$$

$$S_{\mathrm{arm}}^{(2,j)} = -\beta_j^A - \sqrt{3}\gamma_j^A + (\beta_j^B + \sqrt{3}\gamma_j^B)e^{i(q_x+q_{yj})}, \tag{C.2b}$$

$$S_{\mathrm{arm}}^{(3,j)} = \sqrt{3}\beta_j^A - \gamma_j^A - (\sqrt{3}\beta_j^B - \gamma_j^B)e^{i(q_x+q_{yj})}, \tag{C.2c}$$

$$S_{\mathrm{arm}}^{(4,j)} = (2\alpha_j^A - \sqrt{3}\beta_j^A - \gamma_j^A)e^{i(-q_x+q_{yj})} - 2\alpha_j^2 - \sqrt{3}\beta_j^B - \gamma_j^B, \tag{C.2d}$$

$$S_{\mathrm{arm}}^{(5,j)} = (\beta_j^A - \sqrt{3}\gamma_j^A)e^{i(-q_x+q_{yj})} - \beta_j^B + \sqrt{3}\gamma_j^B, \tag{C.2e}$$

$$S_{\mathrm{arm}}^{(6,j)} = (\sqrt{3}\beta_j^A + \gamma_j^A)e^{i(-q_x+q_{yj})} - \sqrt{3}\beta_j^B - \gamma_j^B, \tag{C.2f}$$

where $j = 1, \ldots, 6$.

References

[1] N. Boechler, G. Theocharis, C. Daraio, Nature Mater. 10 (2011) 665–668.
[2] F. Li, P. Anzel, J. Yang, P.G. Kevrekidis, C. Daraio, Nat. Commun. 5 (2014) 5311.
[3] M.A. Porter, P.G. Kevrekidis, C. Daraio, Phys. Today 68 (11) (2015) 44.
[4] A.V. Akimov, Y. Tanaka, A.B. Pevtsov, S.F. Kaplan, V.G. Golubev, S. Tamura, D.R. Yakovlev, M. Bayer, Phys. Rev. Lett. 101 (2008) 033902.
[5] L.M. Schwartz, D.L. Johnson, S. Feng, Phys. Rev. Lett. 52 (1984) 831.
[6] A.S.J. Suiker, A.V. Metrikine, R. de Borst, Int. J. Solids Struct. 38 (2001) 1563–1583.
[7] I.S. Pavlov, A.I. Potapov, G.A. Maugin, Int. J. Solids Struct. 43 (2006) 6194–6207.
[8] H. Muhlaus, F. Oka, Int. J. Solids Struct. 33 (1996) 2841.
[9] H. Pichard, A. Duclos, J.-P. Groby, V. Tournat, V.E. Gusev, Phys. Rev. E 89 (2014) 013201.
[10] S.P. Wallen, A.A. Maznev, N. Boechler, Phys. Rev. B 92 (2015) 174303.
[11] H. Pichard, A. Duclos, J.-P. Groby, V. Tournat, V. Gusev, Phys. Rev. B 86 (2012) 134307.
[12] V. Tournat, I. Perez-Arjona, A. Merkel, V. Sanchez-Morcillo, V. Gusev, New J. Phys. 13 (2011) 073042.
[13] L.-Y. Zheng, H. Pichard, V. Tournat, G. Theocharis, V. Gusev, Ultrasonics 69 (2016) 201–214.
[14] H. Pichard, A. Duclos, J.-P. Groby, V. Tournat, L.-Y. Zheng, V. Gusev, Phys. Rev. E 93 (2016) 023008.
[15] A. Merkel, V. Tournat, V. Gusev, Phys. Rev. E 82 (2010) 031305.
[16] A. Merkel, V. Tournat, V. Gusev, Phys. Rev. Lett. 107 (2011) 225502.
[17] J. Cabaret, P. Béquin, G. Theocharis, V. Andreev, V.E. Gusev, V. Tournat, Phys. Rev. Lett. 115 (2015) 054301.
[18] T. Kariyado, Y. Hatsugai, Sci. Rep. 5 (2015) 18107.
[19] J. Cserti, G. Tichy, European J. Phys. 25 (2004) 723–736.
[20] A.K. Geim, K.S. Novoselov, Nature Mater. 6 (2007) 183–191.
[21] A.H. Castro Neto, F. Guinea, N.M.R. Peres, K.S. Novoselov, A.K. Geim, Rev. Modern Phys. 81 (2009) 109.
[22] S. Das Sarma, S. Adam, E.H. Hwang, E. Rossi, Rev. Modern Phys. 83 (2011) 407.
[23] J. Zak, Phys. Rev. B 32 (1985) 2218.
[24] P. Delplace, D. Ullmo, G. Montambaux, Phys. Rev. B 84 (2011) 195452.
[25] M. Xiao, Z.Q. Zhang, C.T. Chan, Phys. Rev. X 4 (2014) 021017.
[26] M. Fujita, K. Wakabayashi, K. Nakada, K. Kusakabe, J. Phys. Soc. Japan 65 (1996) 1920.
[27] K. Nakada, M. Fujita, G. Dresselhaus, M.S. Dresselhaus, Phys. Rev. B 54 (1996) 17954.
[28] K. Wakabayashi, M. Fujita, H. Ajiki, M. Sigrist, Phys. Rev. B 59 (1999) 8271.
[29] S. Ryu, Y. Hatsugai, Phys. Rev. Lett. 89 (2002) 077002.
[30] S. Ryu, Y. Hatsugai, Physica E 22 (2004) 679–683.
[31] M. Kohmoto, Y. Hasegawa, Phys. Rev. B 76 (2007) 205402.
[32] K. Esaki, M. Sato, M. Kohmoto, B.I. Halperin, Phys. Rev. B 80 (2009) 125405.
[33] J.G. Checkelsky, Lu Li, N.P. Ong, Phys. Rev. Lett. 100 (2008) 206801.
[34] Y. Hatsugai, Phys. Rev. Lett. 71 (22) (1993) 3697(4).
[35] K.S. Novoselov, A.K. Geim, S.V. Morozov, D. Jiang, M.I. Katsnelson, I.V. Grigorieva, S.V. Dubonos, A.A. Firsov, Nature 438 (2005) 197.
[36] Y. Zhang, Y.-W. Tan, H. Stormer, P. Kim, Nature 438 (2005) 201.
[37] C.L. Kane, E.J. Mele, Phys. Rev. Lett. 95 (2005) 226801.
[38] M. Bellec, U. Kuhl, G. Montambaux, F. Mortessagne, Phys. Rev. B 88 (2013) 115437.
[39] W. Zhong, X. Zhang, Phys. Lett. A 375 (2011) 3533–3536.
[40] M.C. Rechtsman, Y. Plotnik, J.M. Zeuner, D. Song, Z. Chen, A. Szameit, M. Segev, Phys. Rev. Lett. 111 (2013) 103901.
[41] M. Bellec, U. Kuhl, G. Montambaux, F. Mortessagne, New J. Phys. 16 (2014) 113023.
[42] T. Ochiai, M. Onoda, Phys. Rev. B 80 (2009) 155103.
[43] X. Ao, Z. Lin, C.T. Chan, Phys. Rev. B 80 (2009) 033105.

Please cite this article in press as: L.-Y. Zheng, et al., Zero-frequency and extremely slow elastic edge waves in mechanical granular graphene, Extreme Mechanics Letters (2016), http://dx.doi.org/10.1016/j.eml.2016.08.003

[44] Z. Yang, F. Gao, X. Shi, X. Lin, Z. Gao, Y. Chong, B. Zhang, Phys. Rev. Lett. 114 (2015) 114301.
[45] X. Ni, C. He, X.C. Sun, X.P. Liu, M.H. Lu, L. Feng, Y.F. Chen, New J. Phys. 17 (2015) 053016.
[46] P. Wang, L. Lu, K. Bertoldi, Phys. Rev. Lett. 115 (2015) 104302.
[47] Y.-T. Wang, P.-G. Luan, S. Zhang, New J. Phys. 17 (2015) 073031.
[48] D. Torrent, J. Sanchez-Dehesa, Phys. Rev. Lett. 108 (2012) 174301.
[49] E. Kalesaki, C. Delerue, C.M. Smith, W. Beugeling, G. Allan, D. Vanmaekelbergh, Phys. Rev. X 4 (2014) 011010.
[50] A.V. Savin, Y.S. Kivshar, Phys. Rev. B 81 (2010) 165418.
[51] L.M. Nasha, D. Klecknera, A. Reada, V. Vitellib, A.M. Turnerc, W.T.M. Irvine, Proc. Natl. Acad. Sci. 112 (47) (2015) 14495–14500.
[52] F. Allein, V. Tournat, V.E. Gusev, G. Theocharis, Appl. Phys. Lett. 108 (2016) 161903.
[53] F. Allein, V. Tournat, V.E. Gusev, G. Theocharis, Extreme Mech. Lett. (2016) http://dx.doi.org/10.1016/j.eml.2016.08.001.
[54] V.F. Nesterenko, Dynamics of Heterogeneous Materials, Springer, 2001.
[55] C. Coste, E. Falcon, S. Fauve, Phys. Rev. E 56 (1997) 6104.
[56] K. Sun, A. Souslov, X. Mao, T.C. Lubensky, Proc. Natl. Acad. Sci. 109 (2012) 12369–12374.
[57] C.L. Kane, T.C. Lubensky, Nat. Phys. 10 (2014) 39–45.
[58] J. Paulose, B.G. Chen, V. Vitelli, Nat. Phys. 11 (2015) 153–156.
[59] X. Mao, N. Xu, T.C. Lubensky, Phys. Rev. Lett. 104 (2010) 085504.
[60] N. Boechler, J.K. Eliason, A. Kumar, A.A. Maznev, K.A. Nelson, N. Fang, Phys. Rev. Lett. 111 (2013) 036103.
[61] M. Hiraiwa, M. Abi Ghanem, S.P. Wallen, A. Khanolkar, A.A. Maznev, N. Boechler, Phys. Rev. Lett. 116 (2016) 198001.

Please cite this article in press as: L.-Y. Zheng, et al., Zero-frequency and extremely slow elastic edge waves in mechanical granular graphene, Extreme Mechanics Letters (2016), http://dx.doi.org/10.1016/j.eml.2016.08.003